Brain states and tau PET patterns interact across the aging-Alzheimer's continuum

Hugo Botha M.B., Ch.B.[1], Jonathan Graff-Radford M.D.[1], Jeffrey L Gunter Ph.D.[1], Val J. Lowe M.D.[1], Scott A. Przybelski B.S.[1], Christopher G. Schwarz Ph.D[1], Matthew L. Senjem M.S.[1], Kejal Kantarci M.D.[1], Bradley F. Boeve M.D.[1], Prashanthi Vemuri Ph.D, David S. Knopman M.D.[1], Ronald C. Petersen M.D., Ph.D.[1], Clifford R. Jack, Jr. M.D.[1], David T. Jones M.D.[1]

[1]Mayo Clinic, Rochester, MN

Objective

Explore the relationship between dynamic brain activity across the age spectrum, biomarker evidence of Alzheimer's disease pathophysiology and cognitive impairment

880 Participants from the Mayo Clinic Study of Aging and the Mayo Alzheimer's Research Center with concurrent fMRI, amyloid PET, tau PET and cognitive testing[1]

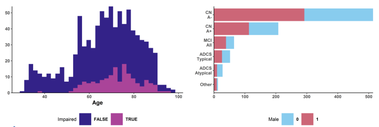

Across cohort independent component analysis[2]

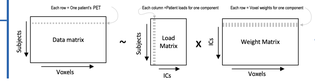

Across cohort hidden markov model based time series segmentation[3]

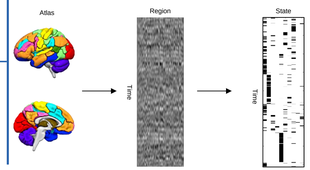

Tau components potentially related to AD[4]

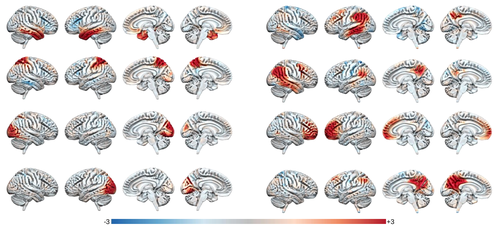

Amyloid components potentially related to AD[4]

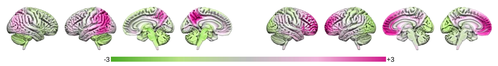

Component based similarity matrix[6] (14 tau, 3 amyloid)

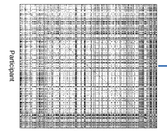

Mean regional activity during state[5]

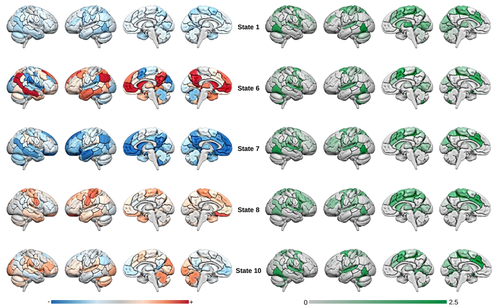

Regional degree centrality during state[5]

Fractional occupancy (dwell time)[7]

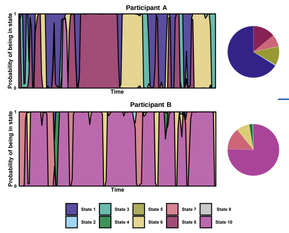

Graph embedding and spectral clustering[8]

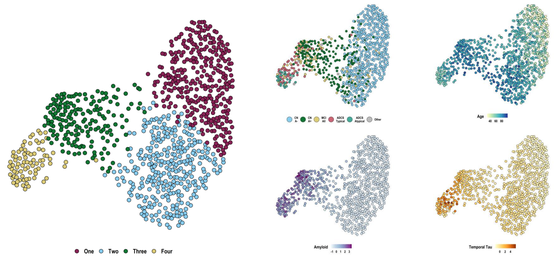

State 1[9]

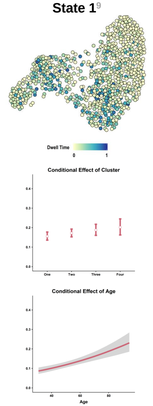

State 8[9]

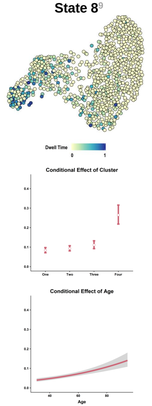

State 10[9]

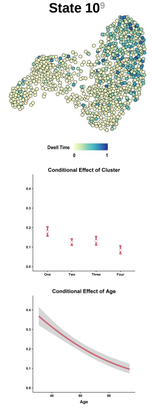

Conclusions

Amyloid and tau PET heterogeneity in aging and AD can be captured by a relatively small set of statistically independent patterns

Similarly, dynamic functional connectivity across healthy aging and the AD spectrum can be captured by a set of distinct brain states

A low dimensional graph embedding based on PET patterns mapped onto age, phenotype and dynamic connectivity

Our findings support a link between AD molecular pathology and dynamic, network level changes

Methodological minutiae

1. **These participants represent a subset of a larger cohort of patients who had concurrent amyloid, tau, fMRI and cognitive testing. We excluded cases with sedation during the fMRI, excessive motion or other artefacts. We also limited the cognitively impaired group to those that were A+, in order to focus on the AD-spectrum**
2. **ICA was performed with the GIFT toolbox using the *InfoMax* ICA algorithm with default settings. We use *ICASSO* function to run the ICA 50 times with random initialization and bootstrap sampling to evaluate the consistency of the components identified. The variance explained, correlation between components (i.e. a measure of their independence) and consistency of components across runs were used to determine the appropriate dimensionality.**
3. **We used the Schaefer 100 atlas and added mesial temporal, deep gray and cerebellar ROIs from the AAL atlas. All patient time series data were concatenated into a large matrix which was then decomposed into latent states using a Hidden Markov Model. The model was run with orders from 4-50 and optimal model order was determined based on minimizing free energy and maximizing the across-participant dynamics explained**
4. **The optimal tau decomposition consisted of 42 components. 14 were potentially related to AD, in that they consisted of high voxel weights primarily in gray matter. The non-AD relevant components included off-target intra-axial binding (white matter, deep gray, brainstem, etc.) or extra-axial uptake (skull, dura, etc.). For amyloid, 7 components were determined to be the optimal dimensionality, and 3 of these were potentially AD related whereas the other 4 consisted off-target/artefactual signal. A subset are shown.**
5. **Ten brain states were present in the optimal decomposition, which differed in terms of regional activity (relatively higher/lower relative to mean) as well as connectivity. A subset are shown.**
6. **Participant loads on the amyloid and tau components potentially related to AD were used to create a high dimensional similarity matrix**
7. **For each fMRI time point (volume), the model outputs a set of state probabilities. This allowed us to calculate the fractional occupancy – or dwell time – for each state, for each patient. Two patient examples are show.**
8. **For directed graph representation with cluster assignment from spectral clustering (left) as well as selected clinical and PET data (right panels) overlaid. Note the age gradient running from top to bottom towards the right of the graph, and the AD-related changes running right to left.**
9. **Dwell times for selected states mapped onto different areas of the graph. Using the clusters, we fit a model in *brms/Stan* predicting dwell time using cluster and age. Conditional effects of cluster and age are shown, revealing that age is the predominant driver of variance in State 1 and 10, whereas dwell time on State 8 is primarily predicted by membership of State 8**